scientific reports

Check for updates

OPEN

Total body irradiation is associated with long-term deficits in femoral bone structure but not mechanical properties in male rhesus macaques

Isabel R. Barnet[2,7]✉, Shannon R. Emerzian[1,2,7], Ramina Behzad[3], Daniel J. Brooks[1,4], Trinity Tedtsen[4], Marcela Granados[1], Sun Park[5], Joseph Moore[5], John D. Olson[6], Lamya Karim[3], Mary L. Bouxsein[1,2], J. Mark Cline[6] & Jeffrey S. Willey[5]

Exposure to ionizing radiation for oncological therapy increases the risk for late-onset fractures in survivors. However, the effects of total body irradiation (TBI) on adult bone are not well-characterized. The primary aim of this study was to quantify the long-term effects of TBI on bone microstructure, material composition, and mechanical behavior in skeletally mature rhesus macaque (*Macaca mulatta*) non-human primates. Femora were obtained post-mortem from animals exposed to an acute dose of TBI (6.0–6.75 Gy) nearly a decade earlier, age-matched non-irradiated controls, and non-irradiated young animals. The microstructure of femoral trabecular and cortical bone was assessed via micro-computed tomography. Material composition was evaluated by measuring total fluorescent advanced glycation end products (fAGEs). Cortical bone mechanical behavior was quantified via four-point bending and cyclic reference point indentation (cRPI). Animals exposed to TBI had slightly worse cortical microstructure, including lower cortical thickness (-11%, $p = 0.037$) and cortical area (-24%, $p = 0.049$), but similar fAGE content and mechanical properties as age-matched controls. Aging did not influence cortical microstructure, fAGE content, or cRPI measures but diminished femoral cortical post-yield properties, including toughness to fracture (-32%, $p = 0.032$). Because TBI was administered after the acquisition of peak bone mass, these results suggest that the skeletons of long-term survivors of adulthood TBI may be resilient, retaining or recovering their mechanical integrity during the post-treatment period, despite radiation-induced architectural deficits. Further investigation is necessary to better understand radiation-induced skeletal fragility in mature and immature bone to improve care for radiation patients of all ages.

Keywords Total body irradiation, Bone, Rhesus macaques, Bone mechanics, Bone microstructure

Total body irradiation (TBI) is known to induce multi-system toxicity, affecting the gastrointestinal, reproductive, vascular, and immune systems[1]. However, the effects of TBI on the skeleton are poorly characterized. Radiation-induced skeletal toxicity is an important clinical concern, as exposure to radiation for cancer treatment increases the risk of fracture for otherwise healthy bones within the radiation treatment field for years following therapy in both adult and childhood cancer patients[2–8]. For example, long-term survivors of pediatric hematopoietic stem cell transplantation given TBI (12–13.2 Gy) experienced a greater number of compression fractures and vertebral deformities at a median of 9.7 years after TBI compared to healthy controls[8]. In comparison, the long-term effects of TBI in adults are less clear, with some studies reporting an increase in fracture incidence, and others showing no difference compared to non-irradiated controls[2,9,10].

In general, the effect of radiation on the non-growing skeleton is not well-understood, in part because mature bone has long been considered a radiation-resistant tissue[11]. Importantly, studies of localized radiation therapy

[1]Center for Advanced Orthopedic Studies, Beth Israel Deaconess Medical Center, Boston, MA 02215, USA. [2]Harvard Medical School, Boston, MA 02115, USA. [3]Department of Bioengineering, University of Massachusetts Dartmouth, Dartmouth, MA 02747, USA. [4]Department of Medicine, Endocrine Unit, Massachusetts General Hospital, Harvard Medical School, Boston, MA 02114, USA. [5]Department of Radiation Oncology, Section on Radiation Biology, Wake Forest University School of Medicine, Winston-Salem, NC 21757, USA. [6]Department of Pathology, Section on Comparative Medicine, Wake Forest University School of Medicine, Winston-Salem, NC 21757, USA. [7]Isabel R. Barnet, Shannon R. Emerzian contributed equally to this work. ✉email: ibarnet@hms.harvard.edu

in adults have demonstrated that radiation is associated with increased risk of fractures, prolonged fracture healing times, and high-rates of non-union[3–5,12,13]. Given this established post-radiation fracture risk, more work must be done to characterize the effects of irradiation in general and TBI in particular in the adult population.

Though skeletal fragility poses a significant burden to patients undergoing radiation therapy, there is an incomplete understanding of how radiation causes an elevated fracture risk, especially in adult, skeletally mature bones. Bone mineral density (BMD) is often used to monitor bone quantity, but studies report conflicting results on changes in BMD following radiation therapy[2,4,6,9]. Likewise, measuring cortical thinning of the ribs, femoral neck, and vertebrae following targeted radiation treatment have generally indicated rapid, dose-dependent losses of bone, but these changes have not been correlated with late fracture[14,15]. Therefore, it is imperative to investigate other key determinants of bone strength besides bone mass, including bone architecture visualized on the microscopic level, termed bone microstructure, mechanical behavior, and material properties.

Preclinical murine models of radiation have demonstrated compromised trabecular and cortical bone microstructure in skeletally-mature bone in the short-term following radiation exposure[16–23]. Within 12 weeks of exposure, TBI in mice compromises bone structure, with lower trabecular bone volume fraction[17,21]. TBI also reduces cortical thickness and area in the short-term[22,23]. While studies have demonstrated that TBI exposure has a consistent adverse effect on bone microstructure early in the post-treatment period in murine models, its impact on bone material and mechanical behavior is not as well understood. Some small-animal studies have observed alterations to bone material following TBI, including accumulation of advanced glycation end products (AGEs)[21]. Others have shown mechanical deficits in trabecular bone due to aging, not TBI, but more work must be done in this space[17,21].

While small animal models have provided great insight, they are limited in their translatability to humans due to differences between human and mouse bone structure, geometry, and mechanical properties[24–26]. However, larger animal models, such as non-human-primates (NHPs), more closely approximate human conditions due to their genetic, physiologic, and anatomical similarities[24,27–31]. For instance, NHPs exhibit extensive Haversian bone structure, characterized by cylindrical osteons, and undergo intracortical remodeling similar to humans[27]. Their greater lifespan also allows for the study of longer-term effects of radiation on bone, which are of increasing relevance as patients survive their radiation therapy for extended durations.

Despite these benefits, NHP models have not been regularly leveraged to explore the effects of TBI on bone. Therefore, the primary aim of this study was to quantify the late effects of TBI on bone quantity, microstructure, material composition, and mechanical behavior in skeletally-mature rhesus macaque (*Macaca mulatta*) non-human primates from the Wake Forest Radiation Late Effects Cohort (RLEC), a group of NHPs that are long-term survivors of total body irradiation[32,33]. A secondary aim was to quantify the effects of age on bone microstructure, material composition, and mechanical behavior, as age is known to independently increase risk of fracture[34]. We hypothesized that both aging and TBI would diminish bone quantity, structure, and mechanical behavior and alter material composition.

Methods

Sample selection and preparation

Whole right femora were obtained post-mortem from male NHPs in the Radiation Late Effects Cohort (RLEC) at the Wake Forest University School of Medicine (WFUSM), a National Institutes of Health and National Institute of Allergy and Infectious Diseases-supported resource[33]. The animals in the RLEC were irradiated using one of two strategies: (1) linear accelerator-derived photons at a nominal mean energy of 2 MeV, delivered at 80 cGy/minute as a split dose given half anterior-posterior and half posterior-anterior; or (2) Cobalt 60-derived gamma irradiation delivered simultaneously, bilaterally at 60 cGy/min. Note that these are potentially lethal doses: the LD 10/30 (dose with 10% mortality at 30 days) for rhesus macaques is ~ 5.5 Gy, the LD 50/30 is ~ 6.7 Gy, and the LD 90/30 is 8 Gy[35]. Surviving animals were subsequently transferred to Wake Forest School of Medicine Center for Comparative Medicine Research for long-term monitoring post-radiation. Irradiation methods, supportive care strategies, and acute effects for many animals donated to this cohort have been recently reported[33,35,36].

Irradiated NHPs selected for this study had consistent TBI doses, ages at treatment, and treatment latencies. TBI NHPs received a median TBI dose of 6.5 Gy at a median age of 9.2 years. Tissues were harvested from TBI NHPs at a median of 9.1 years post-treatment (Fig. 1A), a duration corresponding to approximately 20–30 human years. Age-matched, non-irradiated controls and young, non-irradiated controls, were also selected, creating three experimental groups: TBI, control, and young NHPs. Comorbidities, such as diabetes status, were noted for each NHP. All procedures involving NHPs were approved by the WFUSM Institutional Animal Care and Use Committee. All methods were performed in accordance with relevant guidelines and regulations. WFUSM is accredited by the Association for Assessment and Accreditation of Laboratory Animal Care, International. The project was performed in compliance with the ARRIVE guidelines.

After humane euthanasia (ketamine sedation followed by barbiturate overdose), femora were harvested fresh and frozen at -20℃ until further processing. The timing of euthanasia was decided by either experimental schedule (in the case of young animals), or (in the case of older animals) predetermined trigger criteria defining serious major morbidities such as cancer, diabetes, heart disease, renal failure, or neurologic disease. After dissection, all specimens were wrapped in gauze soaked with 1X phosphate buffered saline (PBS) and stored at -20℃. Through dissection, preparation, imaging, and mechanical testing, femoral specimens experienced three freeze-thaw cycles.

High-resolution peripheral quantitative computed tomography analysis

Femoral trabecular and cortical microstructure were assessed using a high-resolution peripheral quantitative computed tomography (HR-pQCT) system (XtremeCT2, Scanco Medical, Brüttisellen, Switzerland). Following a quality control phantom calibration scan, each femur was scanned with a 32 μm^3 isotropic voxel size (68 kVp

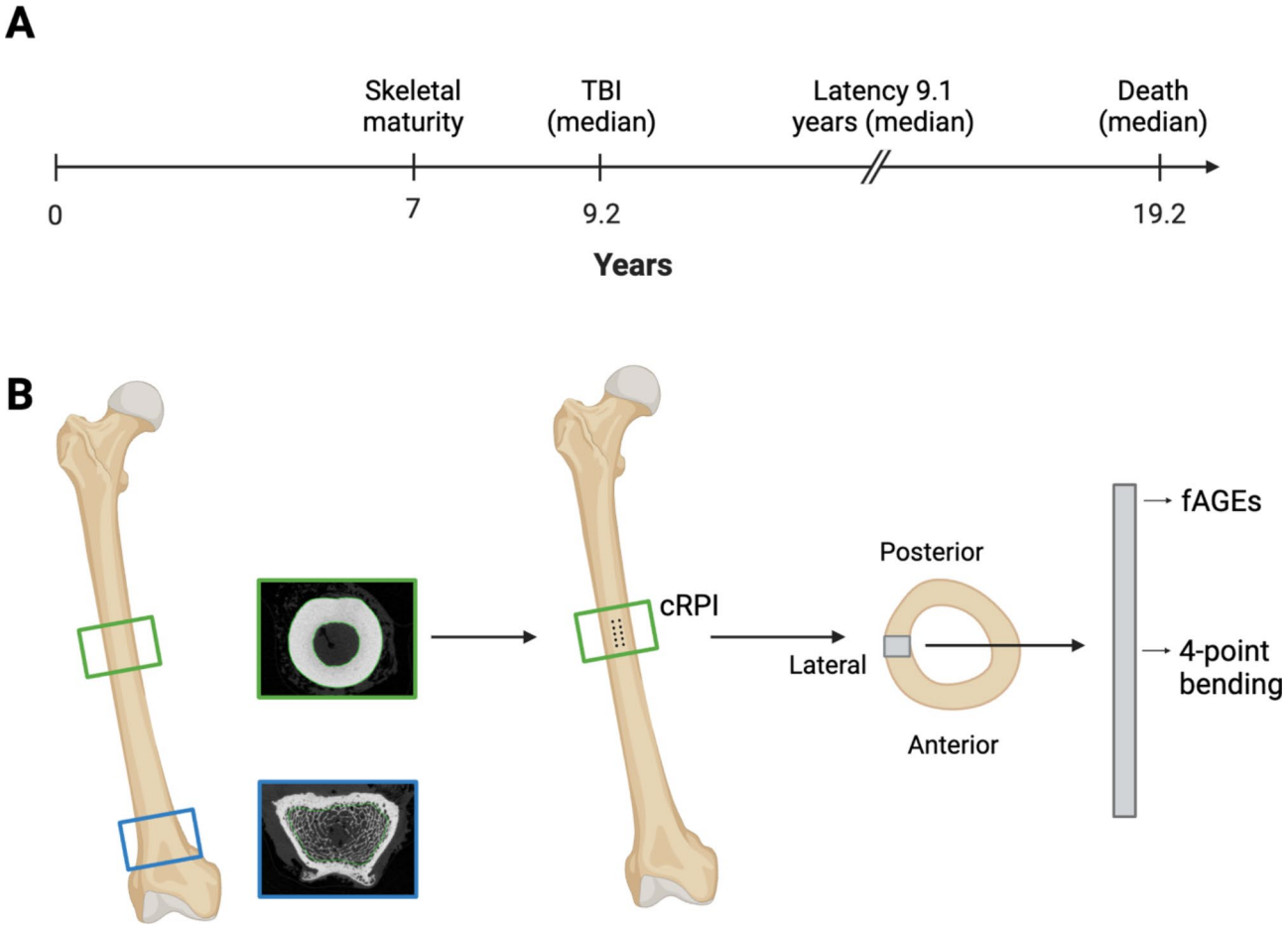

Fig. 1. Overview of the cohort and testing protocol. (**A**) Timeline of non-human primate (NHP) ages and events for total body irradiation (TBI) NHPs. Ages shown on timelines represent medians. Median NHP age at treatment was 9.2 years, and 19.2 years at death. Median post-treatment latency was 9.1 years. (**B**) Femoral trabecular and cortical bone structure were characterized via high-resolution peripheral computed tomography (HR-pQCT) at the mid-shaft (green rectangle; cortical bone) and distal condyles (blue rectangle; trabecular bone). At the mid-shaft, mechanical properties were first evaluated via cyclic reference point indentation (cRPI). Then, one cortical beam (2 × 2 × 40 mm) was extracted from the mid-diaphysis and mechanical properties were evaluated via 4-point bending. After 4-point bending, tissue material composition was characterized by quantifying total fluorescent advanced glycation end products (fAGEs) in the cortical beam. Created in BioRender.com.

peak potential, 1470 µA intensity, 150 ms integration time)[37]. All bone mineral density and microarchitecture measures were calculated using the standard analysis per the manufacturer's standards and published guidelines[37]. The trabecular bone in the resulting image was contoured in a 150-slice region in the distal metaphysis and thresholded at 260 mgHA/cm^3 to measure trabecular bone mineral density (Tb.BMD, mgHA/cm3) and trabecular microstructure (Fig. 1B), including trabecular bone volume fraction (Tb.BV/TV, %), trabecular number (Tb.N, 1/mm), thickness (Tb.Th, mm), separation (Tb.Sp, mm), connectivity density (Conn.D), and structural model index (SMI)[38]. Mid-diaphyseal cortical bone was contoured in a 150-slice region and thresholded at 700 mgHA/cm^3 to measure cortical bone mineral density (Ct.BMD, mgHA/cm^3), cortical tissue mineral density (Ct.TMD, mgHA/cm^3), and cortical microstructure (Fig. 1B), such as cortical thickness (Ct.Th, mm), cortical area (Ct.Ar, mm^2), total cross-sectional area (Tt.Ar, mm^2), and cortical porosity (Ct.Po, %).

Cyclic reference point indentation (cRPI)

The femora were thawed to room temperature and subjected to cyclic reference point indentation (cRPI) tests (BioDent, Active Life Scientific, Santa Barbara, CA). Using BP2 probes, ten indentations (20 cycles at 2 Hz with a peak force of 8 N) were performed approximately 1 mm apart on the anterior surface of the mid-diaphysis (Fig. 1B). The results from the ten separate tests were averaged for each specimen. The following variables were measured with cRPI: indentation distance (ID, µm), creep indentation distance (CID, µm), average creep indentation distance (avg CID, µm), total indentation distance (TID, µm), indentation distance increase (IDI, µm), average energy dissipation (avg ED, µJ), unloading slope (US, N/µm), average unloading slope (avg US, N/µm), and average loading slope (avg LS, N/µm)[39].

Extraction and Preparation of cortical beams

One cortical beam was extracted from the lateral aspect of each femoral mid-diaphysis (Fig. 1B) using a low-speed diamond blade saw (Isomet 1000, Buehler, Lake Bluff, IL) and polished to exact dimensions (2 × 2 × 40 mm) using a specimen polisher (Model 900, South Bay Technologies, Inc., San Clemente, CA) and 12-micron aluminum oxide abrasive film discs (Electron Microscopy Sciences, Hatfield, PA). Beams were wrapped in PBS-soaked gauze and stored at -20 °C until four-point bend testing[39].

Four-point bending

Monotonic four-point bending was performed on the cortical beams using a servohydraulic testing system (Model 8511, Instron, Norwood, MA) with a 220 N load cell. The top and bottom spans of the testing fixture were 9 and 27 mm, respectively, to achieve a 1/3 support span ratio (ASTM D6272–10). The tests were performed with the periosteal surface resting on the bottom supports while the actuator moved at a fixed displacement of 3 mm/min. Force, displacement, and geometry data were used to calculate the estimated mechanical properties of the cortical bone, including bending modulus (E, GPa), yield stress (σ_y, MPa), flexural strength (σ_{ult}, MPa), fracture stress ($\sigma_{fracture}$, MPa), toughness to yield (UYield, mJ/mm^3), toughness to maximum stress (UMax, mJ/mm^3), toughness to fracture (UFrac, mJ/mm^3), and post-yield toughness to fracture (UPY, mJ/mm^3). Yield was defined using a 0.1% offset method.

Total fluorescent Advanced glycation end product (fAGE) quantification

Total fluorescent AGEs (fAGEs) were quantified to determine AGE content in the cortical beams used for mechanical testing. Cortical bone from the proximal end of the cortical beam was isolated, processed into hydroxylates, and diluted 200x for fAGE measurement using previously published methods[39–41]. Using a Synergy HTX Multi-Mode Reader (BioTek, Winooski, VT), fluorescence was measured at 360/460 nm excitation/emission for the diluted hydrolysates and quinine standards. Absorbance was measured at 570 nm for processed hydrolysates and hydroxyproline standards. Collagen content was determined by measuring hydroxyproline quantity in each specimen. Total fAGEs are reported as ng quinine/mg collagen.

Urinary N-Telopeptide analysis

Urinary N-Telopeptide (NTx), a biomarker of bone resorption, was measured from urine samples collected from the bladder at the time of euthanasia to provide insight into osteoclast activity a decade after TBI. Samples were flash frozen in liquid nitrogen and stored at -80 ℃. Samples were thawed, and NTx (nmol BCE/mmol creatinine) was then measured using an ELISA kit (OSTEMARK NTx Urine ELISA, Abbott).

Statistical analysis

Due to the relatively small sample size, group comparisons were made via non-parametric, unpaired Kruskal-Wallis tests or Fisher's tests, as appropriate. If significant differences were detected, Dunn's post-hoc tests were used to assess differences in NHP bone properties due to treatment (control vs. TBI), aging (control vs. young), or the combination of TBI and aging (young vs. TBI). If significant differences were detected, Dunn's post-hoc p-values with Holm-Bonferroni corrections are reported. Statistical analyses were performed using R (version 4.2.1, Vienna, Austria), with the significance level for all tests set to $\alpha \leq 0.05$. Percent differences were calculated between group medians, and data are shown as median (interquartile range).

Results

NHP Cohort

The median age at euthanasia of the TBI, control, and young NHP groups was 19.2 years, 17.2 years, and 9.1 years, respectively. (Fig. 1A; Table 1). Body weight did not vary significantly between groups ($p = 0.075$) but tended to be lower in the TBI group. Finally, compared to control and young NHPs, the TBI group had a greater incidence of diabetes ($p = 0.015$) and tumors at non-skeletal sites ($p = 0.043$), most frequently skin and mesenchymal (sarcoma) tumors. Previous publications in the broader RLEC have demonstrated an increase in tumors, particularly sarcomas, in TBI NHPs compared to non-irradiated controls[31].

Characteristic	Young $N = 6$[1]	Control $N = 9$[1]	TBI $N = 8$[1]	p-value[2]
Age (yrs)	9.1 (9.0, 9.2)	17.2 (15.9, 18.6)	19.2 (17.0, 20.2)	**0.001**
Body Weight (lbs)	19.1 (15.0, 21.1)	14.2 (11.8, 16.4)	12.9 (11.3, 15.5)	0.075
Radiation Dose (Gy)	-	-	6.5 (6.5, 6.5)	-
Age at Radiation (yrs)	-	-	9.2 (8.1, 9.6)	-
Radiation Latency (yrs)	-	-	9.1 (7.2, 12.4)	-
Relevant Conditions				
Diabetes	0 / 6 (0%)	1 / 9 (11%)	5 / 8 (63%)	**0.015**
Tumor	0 / 6 (0%)	0 / 9 (0%)	3 / 8 (38%)	**0.043**

Table 1. NHP cohort characteristics. Data presented as median (IQR); Kruskal-Wallis and Fisher's exact tests assessed group effects. [1] Median (IQR); n / N (%). [2] Kruskal-Wallis rank sum test; Fisher's exact test. Significant values are in bold.

Trabecular microstructure of the distal metaphysis

Trabecular BMD ($p=0.17$) and microstructure ($p>0.08$) of the distal metaphysis were not different across groups (Fig. 2). Tb.BMD, BV/TV, and Tb.N trended slightly lower in control versus young NHPs, though these effects of aging were not significant.

Cortical microstructure of the mid-diaphysis

Compared to the age-similar control group, NHPs exposed to TBI had lower total cross-sectional area (Fig. 3a, Tt.Ar, -24%, $p=0.049$), cortical area (Fig. 3b, Ct.Ar, -24%, $p=0.049$), and cortical thickness (Fig. 3d, Ct.Th, -11%, $p=0.037$) at the femoral mid-diaphysis. TBI-exposed NHPs also had lower total cross-sectional area, cortical area and cortical thickness compared to young animals (-25%, $p=0.019$; -25%, $p=0.019$; -16%, $p=0.006$). While not statistically significant, cortical porosity trended higher in TBI NHPs compared to young NHPs (Fig. 3c, Ct.Po, 60%, $p=0.073$). Cortical tissue mineral density (Fig. 3e, Ct.TMD, -3.66%, $p=0.0086$) was lower in young NHPs compared to TBI NHPs. Cortical bone mineral density (Fig. 3f, Ct.BMD, $p=0.30$) did not differ across groups.

Cortical bone mechanical properties

cRPI

No differences were detected in any cRPI parameter across groups (Table 2**).** Average energy dissipated trended lower in the TBI group compared to control (Table 2, -4.8%, $p=0.11$) and young NHPs (Table 2, -4.5%, $p=0.16$), but these differences did not reach statistical significance.

Four-point bending

Elastic properties, such as bending modulus, did not differ due to aging or TBI (Fig. 4a). Yield stress (Fig. 4b, -11%, $p=0.075$) and toughness to yield (Table 2, -26%, $p=0.19$) trended lower in aged control NHPs compared to young control NHPs, but these group differences did not reach statistical significance. In contrast, post-yield

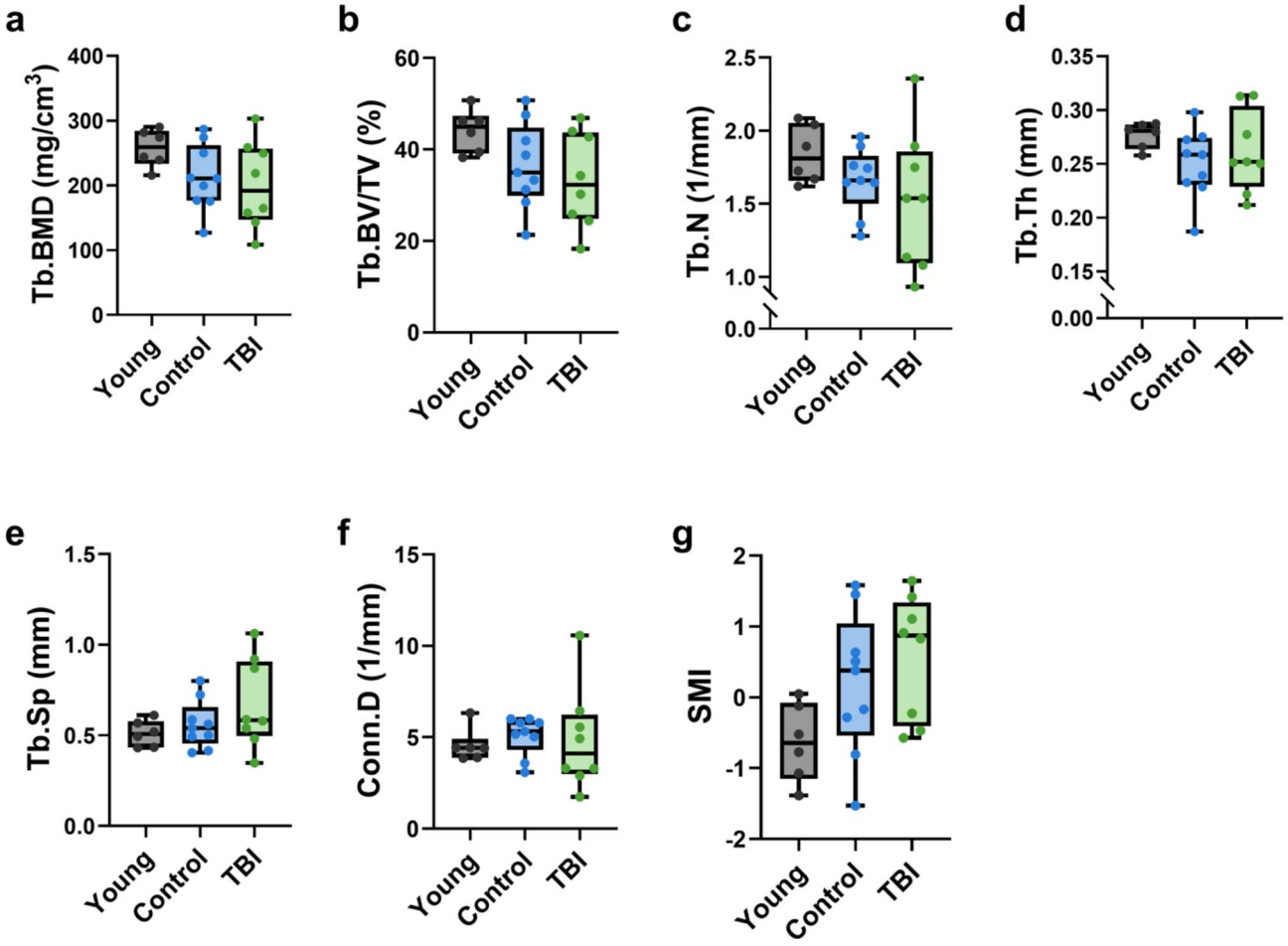

Fig. 2. Femoral trabecular bone mineral density (Tb.BMD) and microarchitecture parameters from the distal metaphysis. Tb.BMD (**a**), trabecular bone volume fraction (Tb.BV/TV, (**b**)), number (Tb.N, (**c**)), thickness (Tb.Th, (**d**)), separation (Tb.Sp, (**e**)), connectivity density (Conn.D, (**f**)), and structural model index (SMI, (**g**)) were not different between groups. Data shown as median ± IQR, with whiskers extended from minimum to maximum.

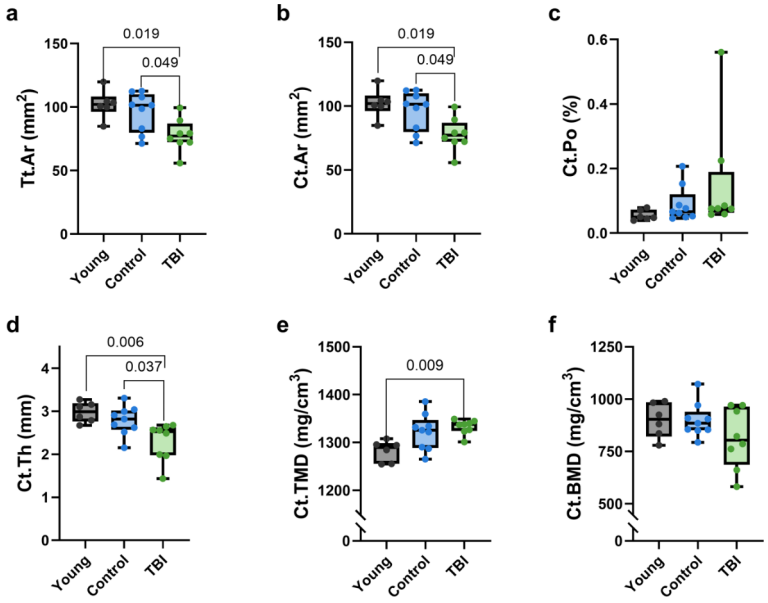

Fig. 3. (**a**-**f**) Tt.Ar, Ct.Ar, Ct.Po, Ct.Th, Ct.TMD, and Ct.BMD of NHP femoral diaphysis. TBI NHPs had lower Tt.Ar (**a**, -24%, $p = 0.049$), Ct.Ar (**b**, -24%, $p = 0.049$), and Ct.Th (**d**, -11%, $p = 0.037$) compared to control NHPs. Ct.Po (**c**) trended higher in TBI NHPs. Data shown as median ± IQR, with whiskers extended from minimum to maximum.

Characteristic	Young $N = 6^1$	Control $N = 9^1$	TBI $N = 8^1$	p-value[2]
Four-Point Bend Parameters				
Apparent Bending Modulus (GPa)	20.1 (18.9, 21.3)	18.6 (17.6, 20.4)	20.9 (18.5, 21.9)	0.412
Yield Stress (MPa)	191 (174, 207)	170 (140, 173)	188 (172, 200)	0.061
Maximum Stress (MPa)	249 (227, 260)	210 (188, 220)	218 (195, 248)	0.057
Fracture Stress (MPa)	172 (167, 184)	162 (91, 178)	157 (113, 194)	0.571
Toughness to Maximum Stress (mJ/mm^3)	4.11 (3.03, 5.49)	2.30 (2.11, 2.54)	2.35 (1.83, 2.74)	0.098
Toughness to Yield (mJ/mm^3)	1.14 (0.95, 1.30)	0.840 (0.760, 0.995)	1.03 (0.970, 1.14)	0.134
Toughness to Fracture (mJ/mm^3)	5.60 (5.06, 6.93)	3.80 (2.63, 4.91)	4.20 (3.38, 4.83)	**0.034**
Post-Yield Toughness (mJ/mm^3)	4.70 (3.92, 5.62)	2.81 (2.06, 3.12)	3.23 (2.36, 3.83)	**0.035**
cRPI Parameters				
Indentation Distance (μm)	60.75 (60.10, 64.93)	62.80 (60.40, 63.60)	61.10 (59.53, 62.75)	0.639
Unloading Slope (N/μm)	0.443 (0.427, 0.454)	0.446 (0.424, 0.465)	0.439 (0.436, 0.459)	0.818
Creep Indentation Distance (μm)	4.40 (4.33, 4.70)	4.60 (4.40, 4.70)	4.45 (4.08, 4.55)	0.714
Total Indentation Distance (μm)	67.1 (65.9, 71.4)	68.8 (66.8, 69.6)	67.5 (65.8, 69.3)	0.809
Indentation Distance Increase (μm)	9.55 (9.32, 9.72)	9.96 (9.03, 10.46)	9.92 (9.35, 10.63)	0.623
Average Creep Indentation Distance (μm)	1.24 (1.21, 1.28)	1.23 (1.19, 1.26)	1.23 (1.19, 1.26)	0.628
Average Energy Dissipated (μJ)	21.36 (20.67, 21.71)	21.42 (21.06, 22.02)	20.39 (19.95, 20.88)	0.077
Average Unloading Slope (N/μm)	0.467 (0.448, 0.477)	0.467 (0.456, 0.505)	0.464 (0.457, 0.475)	0.686
Average Loading Slope (N/μm)	0.378 (0.372, 0.385)	0.378 (0.370, 0.396)	0.375 (0.366, 0.386)	0.665

Table 2. Mechanical properties of NHP femoral cortical bone. Data was gathered via four-point bending and cyclic reference point indentation and is presented as median (IQR). Kruskal-Wallis test assessed group effects. [1] Median (IQR). [2] Kruskal-Wallis rank sum test. Significant values are in bold.

properties, such as toughness to fracture and post-yield toughness, were lower in the control, aged NHPs (Fig. 4c -32%, $p = 0.032$; Fig. 4d, -40%, $p = 0.035$) compared to young NHPs. Maximum stress (Table 2, -16%, $p = 0.05$) and toughness to maximum stress (Table 2, -44%, $p = 0.19$) also trended lower in aged control NHPs versus young NHPs, though these differences were not statistically significant. There were no differences in post-yield properties due to TBI.

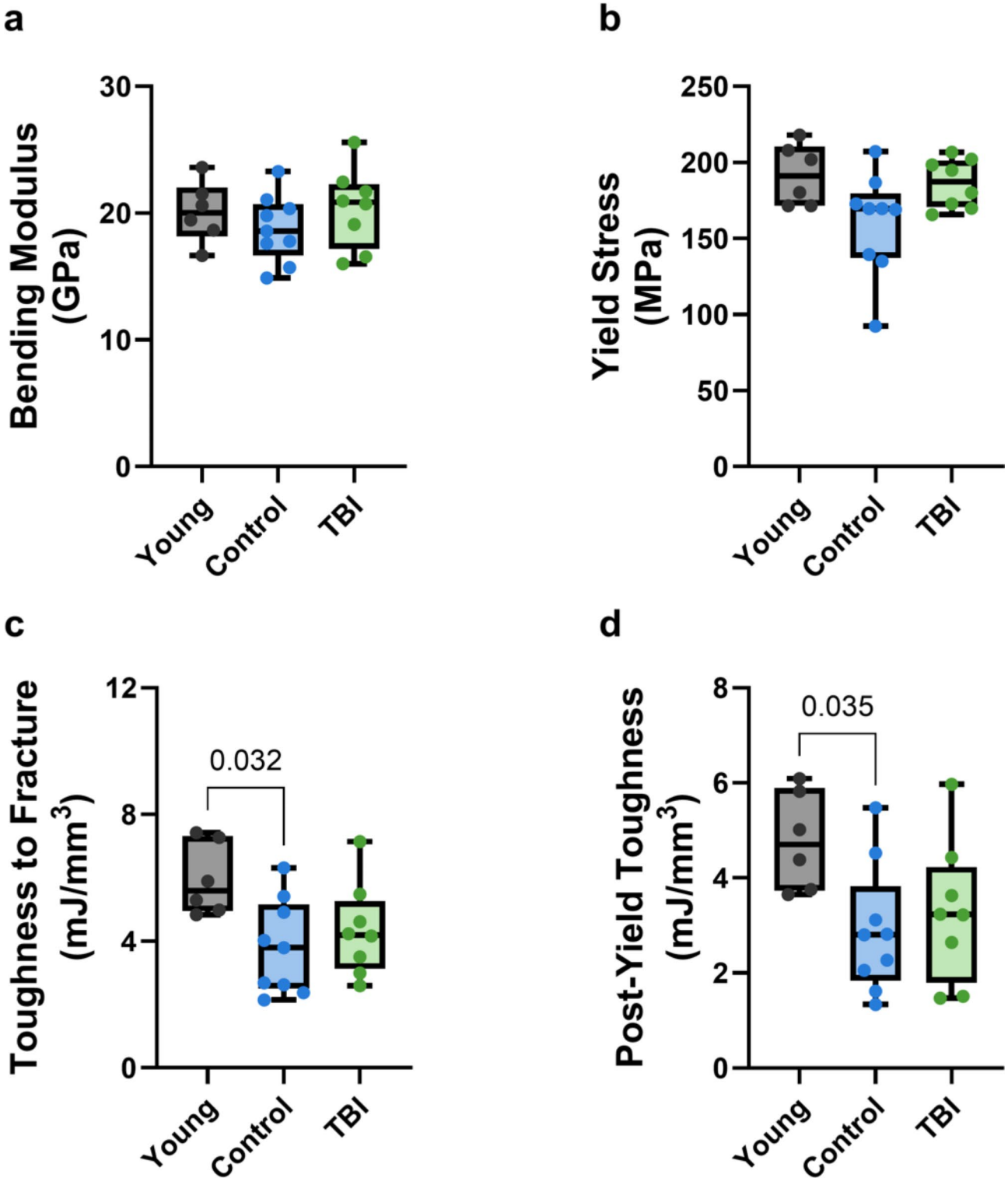

Fig. 4. Elastic (**a,b**) and post-yield (**c,d**) properties of NHP femoral cortical bone. Toughness to fracture and post-yield toughness were lower in control NHPs compared to young NHPs, while bending modulus and yield stress did not differ across any of the groups. Data shown as median ± IQR, with whiskers extended from minimum to maximum.

Total fAGE analysis of femoral cortical bone

Total fAGE (ng quinine/mg collagen) levels did not differ among control (291 [251,311]), TBI (326 [290,378]), and young (309 [274,333]) NHPs ($p=0.21$). Additionally, total fAGE levels were not correlated with elastic or post-yield mechanical properties of the cortical bone.

Urinary N-Telopeptide analysis

NTx levels (nmol BCE/mmol creatinine), measured at the time of euthanasia, were similar in control (718.6 [349.9, 989.7]), TBI (802.7 [561.9, 1044.5], and young (730.0 [449.5, 885.1]) NHPs ($p=0.96$).

Discussion

The purpose of this study was to quantify the long-term effects of total body irradiation (TBI) on cortical bone microstructure and mechanical behavior in skeletally mature rhesus macaques. Approximately a decade after radiation exposure, TBI was associated with mildly diminished femoral mid-diaphyseal cortical bone structure but had no impact on cortical bone material composition or mechanical properties at this site. Aging was associated with deleterious changes in cortical bone post-yield properties, resulting in lower toughness to fracture and post-yield toughness in older versus younger NHPs.

There are many factors that may explain the observed lack of deficit in bone mechanical behavior a decade after TBI treatment. One factor is the TBI dose administered to the NHPs. The 6.5 Gy dose was chosen for the study because it provided a sufficient number of animals with a similar dose for analysis. 6.5 Gy is near the acute LD50/30 for hematopoietic injury after TBI, but it is substantially lower than focal/regional radiotherapy doses, which are typically 40–60 Gy[42,43]. Various studies have shown that post-radiation skeletal consequences are dose-dependent[44–46]. Therefore, the non-human primates exposed to TBI may have retained their skeletal integrity due to the lower-dose exposure in this study, motivating further investigation on the impact of higher doses. Another factor that may influence skeletal response to TBI is the dose regimen. Notably, NHPs were exposed to a single dose of radiation, while both single-fraction and fractionated regimens are used clinically. While single-fraction dosing of total body irradiation for hematopoietic stem cell transplantation has a greater biological effect than fractionated dosing (BED $\alpha/\beta=18$ versus 9), fractionated regimens are favored due to reduced risks of late toxicity[47,48]. However, the incremental differences between daily fractionation and twice-daily, as they compare to single-fraction, are negligible[47,48]. Thus, while it is likely that both the magnitude and regimen of TBI dosing impact the skeletal response, magnitude is likely to play a larger role.

It is also possible that the non-human primates in this study suffered mechanical deficits earlier in the latency period after TBI, but subsequently recovered during over the decade-long post-treatment period. This pattern of recuperation of initial losses following radiation has been demonstrated in some studies[10,49]. For example, Sugimoto et al. showed that initial deficits (at 12 and 24 weeks) in cortical bending strength of rabbit tibias treated with 50 Gy local radiation tended toward recovery by 1-year post-treatment, a duration corresponding to 15–20 human years[20,50]. Moreover, the non-human primates exposed to TBI in this study, treated with a significantly lower dose of total body, not localized, radiation, may have been less impacted by the radiation in the first place and/or more capable of regaining bone mechanical properties within the decade following treatment.

In the current study, exposure to TBI *after* skeletal maturity could also contribute to the lack of difference in bone mechanical properties[44–46], as all of the treated animals received irradiation after achieving peak bone mass, which occurs by about age 7 in male rhesus macaques[51,52]. In clinical studies, TBI administered to children and adolescents prior to skeletal maturity has been shown to interfere with normal bone mass acquisition and growth, elevating these patients' long-term risks of fracture, osteoporosis, short stature, and other skeletal abnormalities[6–8,44–46,53]. Since bone mass acquisition was complete at the time of treatment in the current NHP cohort, perhaps the long-term effects of TBI on bone mechanics were attenuated, less severe, or more recoverable. Importantly, our results demonstrate that TBI after acquisition of peak bone mass may have minimal impact on cortical bone fragility. More broadly, this study suggests that the mechanical properties of the bones of long-term survivors of a single dose of total body radiation in adulthood are resilient, retaining or recovering their mechanical integrity over the decade-long post-treatment latency period.

While four-point bending tests showed deficits in material properties due to aging, we observed no group differences in mechanical properties assessed by cRPI. This is not surprising given the differences between mechanical behavior measured by cRPI versus four-point bending. While cRPI assesses mechanical behavior within localized regions of the bone at the microscale, four-point bending quantifies macroscale or tissue-level mechanical properties. cRPI microscale properties, while informative, do not capture the complex, hierarchical structure of cortical bone tissue or the macroscale tissue-level mechanical behavior. Furthermore, the relationship between cRPI and bone mechanical behavior at the macroscale (cortical tissue) or whole-bone levels is not clear. While one study has demonstrated a negative correlation between rat femur whole bone strength (assessed via 3-point bending) and indentation distance increase obtained from cRPI[54], several other studies have shown no association between cRPI and cortical tissue-level material properties[55,56]. In our study, cRPI and four-point bend measures were not correlated, highlighting the importance of multiscale bone tissue material property characterization.

This study lends interesting insights into the field of aging, as well. Cortical bone post-yield properties were lower in older compared to young NHPs, and TBI did not exacerbate this effect. The dominance of aging, not TBI, in this skeletal response aligns with findings in the TBI mouse model by Pendleton et al.[21] The observed reductions in cortical post-yield properties due to aging have been reported in many previous studies[50,57]. However, many of these studies attribute these post-yield property deficits to the accumulation of advanced glycation end-products. For example, Wang et al. studied the mechanical properties of 30 human cadaveric femurs from donors of various ages and found that age-related decreases in fracture toughness and post-yield

toughness were correlated with adverse changes in the bone collagen network, such as collagen denaturation and accumulation of advanced glycation end products[50]. Nyman et al. also reported that collagen content and nonenzymatic crosslinks explained age-related decreases in post-yield energy dissipation[57]. In our animal model of TBI, total fAGEs were not different between aged control and young NHPs, and they were not correlated with cortical post-yield properties. However, the inherent variation in the fAGE assay and small sample size in the study may have impaired our ability to detect age-related changes. Additionally, the fAGE data is a bulk measurement of overall crosslink fluorescence, but measurement of individual crosslinks, such as pentosidine and carboxymethyl-lysine, may show difference across groups. Ultimately, quantification of these other specific AGEs, as well as a more comprehensive assessment of bone matrix quality via spectroscopy (i.e., Raman spectroscopy or Fourier Transform Infrared Spectroscopy), atomic force microscopy (AFM), or small angle x-ray scattering could provide additional insight into these post-yield deficits due to aging. Basic fuchsin staining could also be employed to visualize the extent of microcracks and microdamage in the cortical bone tissue of NHPs.

The effects of TBI on the NHPs in our study align with those seen in the broader Radiation Late Effects Cohort (RLEC). Kavanagh et al. studied a group of NHPs from the RLEC 5–9 years post-TBI (6.5–8.4 Gy) and reported that the NHPs exposed to TBI were more likely to develop type 2 diabetes and lose visceral fat mass[58]. Similar trends were observed in our study; TBI NHPs disproportionately developed diabetes and also had lower body weights compared to controls. Overall, the alignment between the phenotypes of TBI NHPs in our study with other, larger studies of the RLEC suggests that our study is representative and generalizable, despite small sample sizes.

The development of diabetes is an established late-effect of TBI[58–60]. In a cohort of RLEC NHPs, Kavanagh et al. found that NHPs developed type 2 diabetes 5–9 years following TBI, attributable to inflammation and impaired peripheral tissue response to insulin[58]. Independently of TBI, type 2 diabetes is associated with an increased risk of fracture, but the mechanism remains poorly understood. Altered bone architecture and accumulation of advanced glycation end products that interfere with collagen crosslinks are two proposed mechanisms[61–64]. In our study, TBI led to diabetes in most but not all NHPs, which could theoretically introduce heterogeneity in fAGE content. However, fAGE content did not differ between diabetic and non-diabetic NHPs ($p = 0.263$), nor between aged control and TBI NHPs. Notably, a recent study of over 3000 women with type 2 diabetes showed that poor physical function, not deficient bone microarchitecture or material properties, to be the dominant reason for the increased fracture risk in type 2 diabetes[65]. Altogether, more information is needed to better understand the relationship between TBI, diabetes, and bone material behavior. Nevertheless, our results highlight the intersection of radiation and diabetes, motivating the simultaneous study of these areas.

This study has several limitations. The NHP cohort in this study was entirely male, so an assessment of sex differences could not be made. Female rhesus macaques reach a lower peak bone density than their male counterparts, and do so later in life, so the response of their skeleton to TBI may differ[51]. In addition, this study was cross-sectional, examining NHP bone at a single time point. Intermediate data from the post-treatment latency period or from TBI NHPs that were euthanized at a younger age would augment our understanding of the time course of bone microstructure and mechanical behavior following TBI exposure. Our study also lacks an NHP group that was exposed to TBI *prior* to skeletal maturity, which would lend valuable insights into the importance of the timing of TBI exposure relative to peak bone mass acquisition.

Furthermore, although this study in NHPs provides unique insight into the effects of TBI on the skeleton, it may have been insufficiently powered to detect small differences in bone microstructure and mechanical behavior between TBI and non-irradiated NHPs. However, the study should have had sufficient power to detect clinically relevant group differences in bone structure; it had approximately 80% power to detect a 20% difference in cortical cross-sectional area. Additionally, we restricted our analysis of TBI to the femur, utilizing a singular beam from the posterior region of the femoral diaphysis. While the small size of the NHP femur did not allow for additional cortical beams to be harvested for mechanical testing, all beams were extracted from the same location across experimental groups, providing comparable tissue samples. Cortical bone structure and material properties are heterogenous and could differ within different regions of the diaphysis, but we do not believe additional bone specimens would have appreciably increased our understanding of bone's response to TBI. Finally, while NHPs are frequently utilized in skeletal research due to the anatomic and physiological similarities to humans[48], the absolute effect size reported for this primate model may not directly translate to humans. Notwithstanding, this model provides unique insight into the latent effects of TBI on femoral cortical bone mechanical properties and material composition.

Despite these limitations, this study was novel in its examination of TBI's impact on bone a decade after treatment in a large animal model using both imaging and mechanical testing techniques. The Radiation Late Effects Cohort is a valuable and informative tool for the study of radiation, especially compared to small animal models. Observational studies in adults treated with TBI have provided useful insights but also have notable limitations. For instance, many of these studies follow patients who received TBI conditioning in the setting of hematopoietic stem cell transplantation, and it is difficult to isolate the effects of TBI on bone from the competing impact of adjacent processes, such as underlying diagnosis, chemotherapy, and transplant medications (i.e. steroids). The RLEC uniquely offers actual bone specimens from NHPs treated with TBI, allowing for assessment of radiation-induced skeletal damage through multiple modalities without the confounders present in the human studies. Additionally, the extended post-treatment latency period in the RLEC NHPs is notably longer than most human adult observational studies[9,10], offering novel clinical insights into the implications of TBI for a growing population of long-term cancer survivors.

In conclusion, in our NHP model of TBI, radiation exposure was associated with long-term diminished cortical architecture in the femora but no deficits in the mechanical properties. These results suggest that the femora of long-term survivors of adulthood TBI retain or recover their mechanical integrity over a decade

post-treatment, despite losses in bone architecture. Further investigation is necessary to understand radiation-induced skeletal fragility in mature and immature bone to better inform the care of radiation-therapy patients of all ages.

Data availability

The data presented in this study are available upon reasonable request from the corresponding author.

Received: 29 July 2024; Accepted: 4 October 2024
Published online: 08 October 2024

References

1. Kiang, J. G. & Olabisi, A. O. Radiation: a poly-traumatic hit leading to multi-organ injury. *Cell. Biosci.* **9**, 25 (2019).
2. Stern, J. M. et al. Bone density loss after allogeneic hematopoietic stem cell transplantation: a prospective study. *Biol. Blood Marrow Transpl.* **7**, 257–264 (2001).
3. Baxter, N. N., Habermann, E. B., Tepper, J. E., Durham, S. B. & Virnig, B. A. Risk of pelvic fractures in older women following pelvic irradiation. *JAMA*. **294**, 2587–2593 (2005).
4. Yaprak, G. et al. Osteoporosis development and vertebral fractures after abdominal irradiation in patients with gastric cancer. *BMC Cancer*. **18**, 972 (2018).
5. Cunha, M. V. R. et al. Vertebral compression fracture (VCF) after spine stereotactic body radiation therapy (SBRT): analysis of predictive factors. *Int. J. Radiat. Oncol. Biol. Phys.* **84**, e343–349 (2012).
6. van Atteveld, J. E. et al. Risk and determinants of low and very low bone mineral density and fractures in a national cohort of Dutch adult childhood cancer survivors (DCCSS-LATER): a cross-sectional study. *Lancet Diabetes Endocrinol.* **11**, 21–32 (2023).
7. Jackson, T. J., Mostoufi-Moab, S., Hill-Kayser, C., Balamuth, N. J. & Arkader, A. Musculoskeletal complications following total body irradiation in hematopoietic stem cell transplant patients. *Pediatr. Blood Cancer* **65**, e26905 (2018).
8. Mostoufi-Moab, S. et al. Adverse Fat depots and Marrow Adiposity are Associated with skeletal deficits and insulin resistance in Long-Term survivors of Pediatric hematopoietic stem cell transplantation. *J. Bone Min. Res. Off J. Am. Soc. Bone Min. Res.* **30**, 1657–1666 (2015).
9. Savani, B. N. et al. Increased risk of bone loss without fracture risk in long-term survivors after allogeneic stem cell transplantation. *Biol. Blood Marrow Transpl. J. Am. Soc. Blood Marrow Transpl.* **13**, 517–520 (2007).
10. Gandhi, M. K. et al. Significant and persistent loss of bone mineral density in the femoral neck after haematopoietic stem cell transplantation: long-term follow-up of a prospective study. *Br. J. Haematol.* **121**, 462–468 (2003).
11. Farris, M. K. et al. Bench to Bedside: animal models of Radiation Induced Musculoskeletal toxicity. *Cancers*. **12**, 427 (2020).
12. Chandra, A., Park, S. S. & Pignolo, R. J. Potential role of senescence in radiation-induced damage of the aged skeleton. *Bone*. **120**, 423–431 (2019).
13. Cannon, C. P., Lin, P. P., Lewis, V. O. & Yasko, A. W. Management of radiation-associated fractures. *J. Am. Acad. Orthop. Surg.* **16**, 541–549 (2008).
14. Okoukoni, C. et al. A cortical thickness and radiation dose mapping approach identifies early thinning of ribs after stereotactic body radiation therapy. *Radiother Oncol.* **119**, 449–453 (2016).
15. Okoukoni, C. et al. Early dose-dependent cortical thinning of the femoral neck in anal cancer patients treated with pelvic radiation therapy. *Bone*. **94**, 84–89 (2017).
16. Farris, M. et al. Cortical thinning and structural bone changes in non-human Primates following single fraction whole chest Radiation. *Radiat. Res.* **190**, 63–71 (2018).
17. Kondo, H. et al. Total-body irradiation of postpubertal mice with (137)cs acutely compromises the microarchitecture of cancellous bone and increases osteoclasts. *Radiat. Res.* **171**, 283–289 (2009).
18. Emerzian, S. R. et al. Relative effects of Radiation-Induced changes in Bone Mass, structure, and tissue material on vertebral strength in a rat model. *J. Bone Min. Res. Off J. Am. Soc. Bone Min. Res.* **38**, 1032–1042 (2023).
19. Jia, D., Gaddy, D., Suva, L. J. & Corry, P. M. Rapid loss of bone mass and strength in mice after abdominal irradiation. *Radiat. Res.* **176**, 624–635 (2011).
20. Sugimoto, M. et al. Changes in bone after high-dose irradiation. Biomechanics and histomorphology. *J. Bone Joint Surg. Br.* **73**, 492–497 (1991).
21. Pendleton, M. M. et al. Relations between bone quantity, microarchitecture, and collagen cross-links on mechanics following in vivo irradiation in mice. *JBMR Plus*. **5**, e10545 (2021).
22. Willey, J. S. et al. Bone architectural and structural properties after 56Fe26 + Radiation-Induced changes in Body Mass. *Radiat. Res.* **170**, 201–207 (2008).
23. Farley, A. et al. Unloading-Induced cortical bone loss is exacerbated by low-dose irradiation during a simulated Deep Space Exploration Mission. *Calcif Tissue Int.* **107**, 170–179 (2020).
24. Xia, H. J. & Chen, C. S. Progress of non-human primate animal models of cancers. *Dong Wu Xue Yan Jiu Zool. Res.* **32**, 70–80 (2011).
25. Jerome, C., Hoch, B. & Carlson, C. S. 5 - Skeletal System. in *Comparative Anatomy and Histology (Second Edition)* (eds. Treuting, P. M., Dintzis, S. M. & Montine, K. S.) 67–88Academic Press, San Diego, doi: (2018). https://doi.org/10.1016/B978-0-12-802900-8.00005-1
26. Jilka, R. L. The relevance of mouse models for investigating age-related bone loss in humans. *J. Gerontol. Biol. Sci. Med. Sci.* **68**, 1209–1217 (2013).
27. Colman, R. J. Non-human primates as a model for aging. *Biochim. Biophys. Acta BBA - Mol. Basis Dis.* **1864**, 2733–2741 (2018).
28. Pope, N. S., Gould, K. G., Anderson, D. C. & Mann, D. R. Effects of age and sex on bone density in the rhesus monkey. *Bone*. **10**, 109–112 (1989).
29. Rogers, J. & Gibbs, R. A. Comparative primate genomics: emerging patterns of genome content and dynamics. *Nat. Rev. Genet.* **15**, 347–359 (2014).
30. Messaoudi, I., Estep, R., Robinson, B. & Wong, S. W. Nonhuman Primate models of Human Immunology. *Antioxid. Redox Signal.* **14**, 261–273 (2011).
31. Sills, W. S. et al. Total-body irradiation is Associated with increased incidence of mesenchymal neoplasia in a Radiation Late effects Cohort of Rhesus macaques (Macaca mulatta). *Int. J. Radiat. Oncol. Biol. Phys.* **113**, 661–674 (2022).
32. Radiation Late Effects Cohort. *Wake Forest University School of Medicine* https://school.wakehealth.edu/research/labs/j-mark-cline-lab/radiation-late-effects-cohort
33. Farese, A. M. et al. A Nonhuman Primate Model of the hematopoietic Acute Radiation Syndrome Plus Medical Management. *Health Phys.* **103** https://doi.org/10.1097/HP.0b013e31825f75a7 (2012).
34. Ensrud, K. E. Epidemiology of fracture risk with advancing age. *J. Gerontol. Biol. Sci. Med. Sci.* **68**, 1236–1242 (2013).
35. MacVittie, T. J., Farese, A. M. & Jackson, W. The hematopoietic syndrome of the Acute Radiation Syndrome in Rhesus macaques: a systematic review of the Lethal Dose Response Relationship. *Health Phys.* **109**, 342–366 (2015).

36. Yu, J. Z. et al. Subject-based versus Population-Based Care after Radiation exposure. *Radiat. Res.* **184**, 46–55 (2015).
37. Whittier, D. E. et al. Guidelines for the assessment of bone density and microarchitecture in vivo using high-resolution peripheral quantitative computed tomography. *Osteoporos. Int. J. Establ Result Coop. Eur. Found. Osteoporos. Natl. Osteoporos. Found. USA*. **31**, 1607–1627 (2020).
38. Bouxsein, M. L. et al. Guidelines for assessment of bone microstructure in rodents using micro–computed tomography. *J. Bone Min. Res.* **25**, 1468–1486 (2010).
39. Merlo, K. et al. In Vitro-Induced High Sugar environments deteriorate human cortical bone Elastic Modulus and Fracture Toughness. *J. Orthop. Res. Off Publ Orthop. Res. Soc.* **38**, 972–983 (2020).
40. Viguet-Carrin, S., Gineyts, E., Bertholon, C. & Delmas, P. D. Simple and sensitive method for quantification of fluorescent enzymatic mature and senescent crosslinks of collagen in bone hydrolysate using single-column high performance liquid chromatography. *J. Chromatogr. B.* **877**, 1–7 (2009).
41. Vaidya, R. et al. Accumulation of fluorescent advanced glycation end products and carboxymethyl-lysine in human cortical and trabecular bone. *Bone Rep.* **17**, 101634 (2022).
42. Quast, U. Whole body radiotherapy: a TBI-guideline. *J. Med. Phys. Assoc. Med. Phys. India*. **31**, 5–12 (2006).
43. Total body irradiation. A practical review. https://appliedradiationoncology.com/articles/total-body-irradiation-a-practical-review
44. Sanders, J. E. et al. Growth and development following marrow transplantation for leukemia. *Blood*. **68**, 1129–1135 (1986).
45. Cohen, A. et al. Final height of patients who underwent bone marrow transplantation for hematological disorders during childhood: a study by the Working Party for Late Effects-EBMT. *Blood*. **93**, 4109–4115 (1999).
46. Couto-Silva, A. C. et al. Bone markers after total body irradiation in childhood. *Bone Marrow Transpl.* **45**, 437–441 (2010).
47. Sabloff, M., Tisseverasinghe, S., Babadagli, M. E. & Samant, R. Total body irradiation for hematopoietic stem cell transplantation: what can we agree on? *Curr. Oncol. Tor. Ont.* **28**, 903–917 (2021).
48. Brommage, R. Perspectives on using nonhuman primates to understand the etiology and treatment of postmenopausal osteoporosis. *J. Musculoskelet. Neuronal Interact.* **1**, 307–325 (2001).
49. Uezono, H. et al. Pelvic insufficiency fracture after definitive radiotherapy for uterine cervical cancer: retrospective analysis of risk factors. *J. Radiat. Res. (Tokyo)*. **54**, 1102–1109 (2013).
50. Wang, X., Shen, X., Li, X. & Agrawal, C. M. Age-related changes in the collagen network and toughness of bone. *Bone*. **31**, 1–7 (2002).
51. Cerroni, A. M., Tomlinson, G. A., Turnquist, J. E. & Grynpas, M. D. Bone mineral density, osteopenia, and osteoporosis in the rhesus macaques of Cayo Santiago. *Am. J. Phys. Anthropol.* **113**, 389–410 (2000).
52. Mattison, J. A. & Vaughan, K. L. An overview of nonhuman primates in aging research. *Exp. Gerontol.* **94**, 41–45 (2017).
53. Bushhouse, S., Ramsay, N. K., Pescovitz, O. H., Kim, T. & Robison, L. L. Growth in children following irradiation for bone marrow transplantation. *Am. J. Pediatr. Hematol. Oncol.* **11**, 134–140 (1989).
54. Gallant, M. A., Brown, D. M., Organ, J. M., Allen, M. R. & Burr, D. B. Reference-point indentation correlates with bone toughness assessed using whole-bone traditional mechanical testing. *Bone*. **53**, 301–305 (2013).
55. Abraham, A. C., Agarwalla, A., Yadavalli, A., Liu, J. Y. & Tang, S. Y. Microstructural and compositional contributions towards the mechanical behavior of aging human bone measured by cyclic and impact reference point indentation. *Bone*. **87**, 37–43 (2016).
56. Krege, J. B. et al. Reference point indentation is insufficient for detecting alterations in traditional mechanical properties of bone under common experimental conditions. *Bone*. **87**, 97–101 (2016).
57. Nyman, J. S. et al. Age-related factors affecting the postyield energy dissipation of human cortical bone. *J. Orthop. Res.* **25**, 646–655 (2007).
58. Kavanagh, K. et al. Type 2 diabetes is a delayed late effect of whole-body irradiation in Nonhuman Primates. *Radiat. Res.* **183**, 398–406 (2015).
59. van Nimwegen, F. A. et al. Risk of diabetes mellitus in long-term survivors of Hodgkin lymphoma. *J. Clin. Oncol. Off J. Am. Soc. Clin. Oncol.* **32**, 3257–3263 (2014).
60. Holmqvist, A. S. et al. Adult life after childhood cancer in Scandinavia: diabetes mellitus following treatment for cancer in childhood. *Eur. J. Cancer Oxf. Engl. 1990*. **50**, 1169–1175 (2014).
61. Karim, L. et al. Bone microarchitecture, biomechanical properties, and advanced glycation end-products in the proximal femur of adults with type 2 diabetes. *Bone*. **114**, 32–39 (2018).
62. Romero-Díaz, C., Duarte-Montero, D., Gutiérrez-Romero, S. A. & Mendivil, C. O. Diabetes and bone fragility. *Diabetes Ther.* **12**, 71–86 (2021).
63. Moseley, K. F. Type 2 diabetes and bone fractures. *Curr. Opin. Endocrinol. Diabetes Obes.* **19**, 128–135 (2012).
64. Hunt, H. B. et al. Altered tissue composition, microarchitecture, and mechanical performance in Cancellous Bone from men with type 2 diabetes Mellitus. *J. Bone Min. Res.* **34**, 1191–1206 (2019).
65. Zoulakis, M., Johansson, L., Litsne, H., Axelsson, K. & Lorentzon, M. Type 2 diabetes and fracture risk in Older Women. *JAMA Netw. Open.* **7**, e2425106 (2024).

Acknowledgements

This work was supported by National Institutes of Health awards U01AI150578, U19AI67798, T32AG023480 and The Raben Professorship.

Author contributions

IRB: Formal analysis, Investigation, Visualization, Methodology, Writing – original draft, Writing – review & editing. SRE: Conceptualization, Formal analysis, Supervision, Funding acquisition, Investigation, Visualization, Methodology, Writing – original draft, Writing – review & editing. RB: Investigation, Writing – review & editing. DJB: Methodology, Writing – review & editing. TT: Investigation, Writing – review & editing. MG: Investigation, Writing – review & editing. SP: Writing – review & editing. JM: Writing – review & editing, JDO: Investigation, Writing – review & editing. LK: Supervision, Resources, Writing – review & editing. MLB: Conceptualization, Resources, Supervision, Writing – original draft, Writing – review & editing. JMC: Resources, Writing – review & editing. JSW: Resources, Supervision, Funding acquisition, Writing – original draft, Writing – review & editing. All authors participated in final approval of the article.

Declarations

Competing interests

The authors declare no competing interests.

Additional information

Correspondence and requests for materials should be addressed to I.R.B.

Reprints and permissions information is available at www.nature.com/reprints.

Publisher's note Springer Nature remains neutral with regard to jurisdictional claims in published maps and institutional affiliations.